Combined electrical and magneto-optical measurements of the magnetization reversal process at a domain wall trap.

Huang T. Zeng, D. Read, D. Petit, A. V. Jausovec, L. O'Brien et al.

Related Articles

Single-layer behavior and slow carrier density dynamic of twisted graphene bilayer
Appl. Phys. Lett. 100, 091601 (2012)

Growth and surface potential characterization of Bi2Te3 nanoplates
AIP Advances 2, 012114 (2012)

Electron tunneling through atomically flat and ultrathin hexagonal boron nitride
Appl. Phys. Lett. 99, 243114 (2011)

Electrical conductivity of platinum-implanted polymethylmethacrylate nanocomposite
J. Appl. Phys. 110, 114905 (2011)

Electron and hole scattering in short-period InGaAs/InP superlattices
J. Appl. Phys. 110, 073706 (2011)

Additional information on Appl. Phys. Lett.

Journal Homepage: http://apl.aip.org/
Journal Information: http://apl.aip.org/about/about_the_journal
Top downloads: http://apl.aip.org/features/most_downloaded
Information for Authors: http://apl.aip.org/authors

ADVERTISEMENT

Combined electrical and magneto-optical measurements of the magnetization reversal process at a domain wall trap.

Huang T. Zeng,[a] D. Read, D. Petit, A. V. Jausovec, L. O'Brien, E. R. Lewis, and R. P. Cowburn
Department of Physics, Imperial College London, Prince Consort Road, London, London SQ7 2AZ, United Kingdom

We have performed combined electrical and magneto-optical Kerr effect measurements on Permalloy nanowires containing artificial symmetric protrusions. This has enabled us to construct a detailed picture of the energy landscape of such a trap, in excellent agreement with predictions based on recent results. In addition with the aid of micromagnetic simulations, we demonstrate how variations in the observed resistance with respect to the applied field can give us insight into the entire depinning and nucleation processes at domain wall traps. © *2009 American Institute of Physics*. [DOI: 10.1063/1.3098359]

Magnetic domain wall (DW) traps have attracted much recent attention for their applicability in solid-state data storage devices.[1–4] These traps consist of artificial defects in the form of notches or protrusions along a nanowire, which locally increase the propagation field of the DW. Such traps can act as diodes to enable unidirectional motion of oppositely charged DWs under an applied field,[5] or filters that only allow DWs of a given chirality (defined as the sense of rotation of the spins within the DW core) to pass through.[6] More complicated geometries enable logic operations to be performed.[7] Recent experiments have shown that the exact nature of the interaction between the DW and the trap depends on the DW configuration as well as the trap geometry.[8] To fully understand DW-trap interactions, one needs to study both the switching of domains adjacent to the trap, as well as the local magnetization changes as the DW interacts with the trap itself. One possible approach would be via spatially resolved electrical measurements using multiple contacts along the device to measure the anisotropic magnetoresistance (AMR) changes associated with a DW.[9,10] We present here an alternative method using combined magneto-optical Kerr effect (MOKE) and single-point magnetoresistance (MR) at the trap to study the interaction of DWs with a symmetric protrusion in a Permalloy (Py) nanowire. The addition of the MOKE allows us to relate magnetization reversal in the nanowire with MR changes at the trap, enabling better interpretation of the MR data. From this, we constructed the potential energy profile of the trap, confirming predictions based on recent work in the field.[8] We further illustrate how the combined MR and MOKE data allow us to access the full micromagnetic information about the DW depinning and nucleation process at the trap.

The nanowires are fabricated via electron beam lithography on a Si substrate, followed by thermal evaporation of Py and lift-off. The resulting wires are 150 nm wide and 10 nm thick. For such dimensions, we obtain transverse DWs.[11] The wires are L-shaped, with a DW trap halfway along the horizontal arm. The field needed to propel a DW along a straight nanowire without traps is the propagation field (H_P). The field needed to push the DW through the trap and reverse the

magnetization beyond is the transmission field (H_T). Figure 1(a) shows a high-magnification image of a typical trap, consisting of a symmetric protrusion 150 nm wide and extending 60 nm on either side of the wire. Electrical connections to the nanostructure are made via Ti/Au (2 nm/150 nm) contacts in a four-terminal setup, with the voltage contacts located 750 nm on either side of the trap [Figs. 1(b)]. The L-shape of the wire enables us to create DWs via a saturating field along the 45° axis bisecting the corner. This DW is then pushed toward the trap by a horizontal field H_X that reaches a maximum of H_{Push} before reversing and pulling the DW back toward the corner. By changing H_{Push} and measuring the pull field H_{Pull}, we can deduce the potential profile at the trap [see Fig. 1(c) and Ref. 8 for more details].

For the AMR measurement, a low current density of approximately 10^5 A cm^{-2} is used to minimize spin transfer torque effects. The MR signal is dependent on the relative orientation (θ) between the local magnetic moments and the current direction, with the resistivity given by

$$\rho = \rho_\perp + (\rho_\parallel - \rho_\perp)\cos^2 \theta, \tag{1}$$

where $\rho_\parallel$ and $\rho_\perp$ are the respective resistivities when the moments are aligned parallel and perpendicular to the current direction. For Py $\rho_\parallel > \rho_\perp$, so that a transverse DW lowers the net resistance.[12,13] We define the AMR ratio to be $\Delta\rho/\rho_\parallel = \rho_\perp - \rho_\parallel/\rho_\parallel$. MOKE measurements are taken by positioning the laser spot before or after the trap. A dual-channel electronic acquisition system records the MOKE and AMR signals and averages across multiple field cycles to reduce
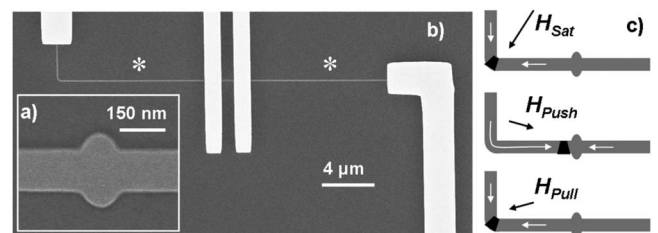

FIG. 1. (a) Typical SEM image of a DW trap. (b) Arrangement of four-terminal electrical contacts on the L wire. The MOKE laser spot is placed at positions denoted by asterisk (*). The central pair of contacts lie on either side of the DW trap. (c) Schematic illustrating the push-pull field sequence.

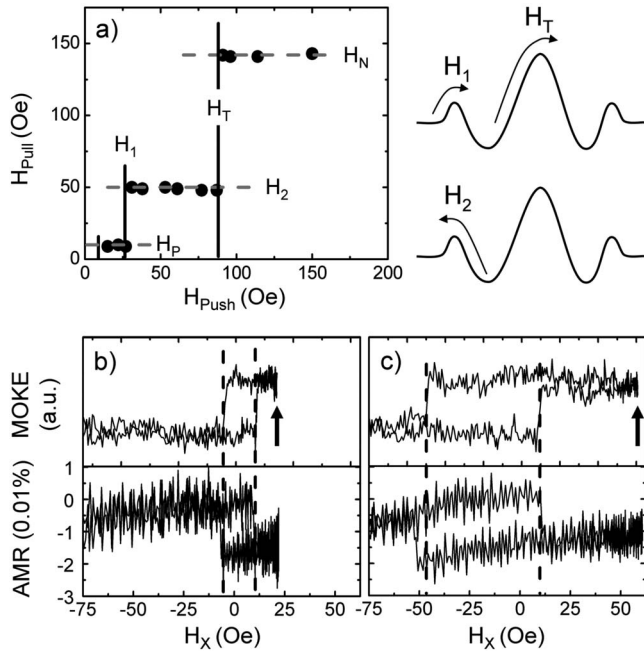[a] Electronic mail: huang.zeng@imperial.ac.uk.

FIG. 2. (a) Push-pull plot for the symmetric protrusion, along with the associated potential profile. H_P is the propagation field along a straight nanowire, H_T is the transmission field needed to push the DW through the trap, and H_N is the nucleation field for creating new walls. The DW needs a field of H_1 to overcome the potential side-barrier and H_2 to be pulled out of the side-well. (b) MOKE and AMR data as a function of H_X for H_{Push} =21 Oe ($H_{Push} < H_1$) and (c) H_{Push}=60 Oe ($H_1 < H_{Push} < H_T$). The arrows indicate the field position of H_{Push}.
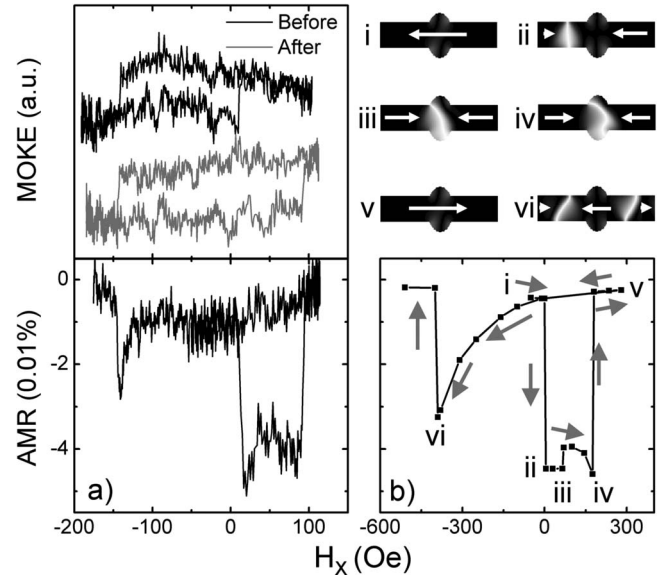

FIG. 3. (a) Experimental AMR and MOKE data for the DW transmission process. The MOKE loops are taken with the laser spot placed both before and after the trap. (b) Simulated AMR as a function of applied field. The arrows indicate time evolution, starting at (i) when the DW approaches the trap. The annotations show the micromagnetic configuration of the region around the trap based on OOMMF simulations.

noise. The acquisition can be done in two modes: in the first mode, individual cycles of MOKE and AMR signals are recorded simultaneously and then averaged; in the second mode, the MOKE and AMR cycles are acquired and averaged consecutively. The second mode takes longer, but has the advantage of extinguishing the laser beam during the electrical measurement. This is important for samples fabricated on a photoconductive substrate such as high resistivity silicon. All the results presented here used the second acquisition mode, with 50 cycles of averaging per signal type.

From Ref. 8, we expect a transverse DW to encounter a simple potential barrier for an asymmetric protrusion located on the narrow side of the DW core, and a potential well for a protrusion on the wide side. For the symmetric protrusion, it is not immediately obvious what the energy landscape will be, since the relative orientation of the DW no longer matters, and the trap offers the same reaction to both chiralities. However, since the symmetric case combines both pinning configurations, we would predict the resultant potential to be a superposition of a central barrier with a central well, giving a complex energy landscape involving a central barrier with side wells and side barriers (see sketch in Fig. 2). Figure 2(a) shows the experimental H_{Pull} versus H_{Push} plot for the device. The results fall into three regimes. For $H_{Push} < H_1$, H_{Pull} =H_P, indicating pinning at a side barrier, which the DW overcomes when $H_{Push} > H_1$. For $H_1 < H_{Push} < H_T$, H_{Pull}=H_2. That $H_2 > H_P$ indicates the DW is stuck in a potential well. Finally for $H_{Push} > H_T$, the DW is pushed through the trap and annihilated at the end of the wire. The nanowire is now a single domain, and a very large, negative H_{Pull} is needed to reverse the magnetization via the nucleation of new DWs at the nucleation field (H_N). The experimental H_{Pull} versus

H_{Push} data agree with the predicted profile for the symmetric protrusion, and shows how the pinning potential of complex traps can be understood via the superposition of potentials for simpler trap geometries. Figures 2(b) and 2(c) show the resistance and MOKE data versus H_X. For H_{Push}=21 Oe [Fig. 2(b)], the AMR and MOKE transitions both occur at ± 9 Oe, which is the propagation field (H_P). Here, the DW depins from the corner and reverses the horizontal arm before the trap, but cannot overcome the side barrier (H_{Push} $< H_1$=27 $\pm$ 2 Oe). It is pinned beside trap until H_X reverses at $-H_P$. Figure 2(c) shows the same data for H_{Push}=60 Oe, when the DW now enters the trap. Since H_T=88 $\pm$ 2 Oe, this is insufficient to transmit the DW through the central barrier and it is pulled back out of the side well when H_X reverses past -51 ± 3 Oe(H_2).

For the case when $H_{Push} > H_T$, the combined MOKE and MR technique reveal the exact micromagnetic details of the transmission and nucleation process, which cannot be ascertained using MOKE alone. Figure 3(a) shows the results for H_{Push}=115 Oe, with the laser spot placed both before and after the DW trap. Following the time development of H_X, the MR begins in a high resistance state until H_X reaches 8 Oe, when a jump to a low resistance state indicates the propagation of the DW into the pinning site. This agrees with the positive field transition in the MOKE loop taken before the trap. The 87 Oe jump back up to the high resistance state corresponds to DW transmission out of the pinning site, and agrees with the positive field transition in the MOKE loop acquired after the trap. The nanowire is now single-domain, and H_X reverses to negative values after reaching H_{Push}. During reversal, the MR signal decreases gradually until -140 Oe when it jumps back to a high state. These local magnetic changes at the trap as measured by the MR is matched by large scale domain reversal seen in the MOKE, giving us insight into the nucleation process. The gradual fall in the MR level preceding the jump implies a continuous rotation

of spins within the trap away from the easy axis. Past a critical angle, a new domain at the trap, the boundaries of which are defined by a pair of DWs. Since the sign of H_X causes this domain to grow, the DWs propagate in opposite directions and reverse the nanowire before and after the trap, which is detected by the MOKE. Comparing our MR results with OOMMF (Ref. 14) simulations on a nominally identical structure [$M_S = 800 \times 10^3$ A/m, $A = 13 \times 10^{-12}$ J/m, and (5,5,5) nm cell size] provides further confirmation. From the simulated data, we were able to numerically compute the MR signal at the trap under applied fields, using the experimentally obtained AMR ratio of -0.7%. Comparing the bottom panel of Figs. 3(a) and 3(b), we see all the key features in experimental MR signal mirrored in the simulated data, from small details, such as the DW overcoming the side barrier at low push fields [(ii)–(iii)], to the major events such as the DW distorting and transmitting through the pinning site [(iii)–(v)]. Clearly the MR results play a key role in unlocking the detailed micromagnetic behavior of the DW as it interacts with traps. One feature to note is the amplitudes of the experimental H_P, H_T, etc. are all approximately 0.35–0.45 times that of simulations. Such differences are expected since the depinning of DWs from wells and barriers is a thermally activated process,[15] but the simulations ignore thermal effects.

In conclusion, we have performed a detailed study of the DW depinning process from a symmetric protrusion by combining MOKE and AMR measurements on the same apparatus and characterized the potential profile of such a trap. By analyzing our experimental observations and making suitable comparisons with simulated MR, we have been able to achieve a full understanding of the depinning and nucleation processes at the trap. This demonstrates this technique to be an ideal *in situ* probe of the micromagnetics of a nanoscale system.

[1] D. A. Allwood, G. Xiong, M. D. Cooke, C. C. Faulkner, D. Atkinson, N. Vernier, and R. P. Cowburn, Science **296**, 2003 (2002).
[2] M. Hayashi, L. Thomas, R. Moriya, C. Rettner, and S. S. P. Parkin, Science **320**, 209 (2008).
[3] S. S. P. Parkin, M. Hayashi, and L. Thomas, Science **320**, 190 (2008).
[4] D. Atkinson, D. S. Eastwood, and L. K. Bogart, Appl. Phys. Lett. **92**, 022510 (2008).
[5] D. A. Allwood, G. Xiong, and R. P. Cowburn, Appl. Phys. Lett. **85**, 2848 (2004).
[6] E. R. Lewis, D. Petit, A. V. Jausovec, L. O'Brien, D. E. Read, H. T. Zeng, and R. Cowburn, Phys. Rev. Lett. **102**, 057209 (2009).
[7] D. A. Allwood, G. Xiong, C. C. Faulkner, D. Atkinson, D. Petit, and R. P. Cowburn, Science **309**, 1688 (2005).
[8] D. Petit, A. V. Jausovec, D. Read, and R. P. Cowburn, J. Appl. Phys. **103**, 114307 (2008).
[9] M. Klaui, C. A. F. Vaz, W. Wernsdorfer, E. Bauer, S. Cherifi, S. Heun, A. Locatelli, G. Faini, E. Cambril, L. J. Heyderman, and J. A. C. Bland, Physica B **343**, 343 (2004).
[10] M. Klaui, C. A. F. Vaz, J. Rothman, J. A. C. Bland, W. Wernsdorfer, G. Faini, and E. Cambril, Phys. Rev. Lett. **90**, 097202 (2003).
[11] Y. Nakatani, A. Thiaville, and J. Miltat, J. Magn. Magn. Mater. **290–291**, 750 (2005).
[12] T. R. McGuire and R. I. Potter, IEEE Trans. Magn. **11**, 1018 (1975).
[13] R. I. Potter, Phys. Rev. B **10**, 4626 (1974).
[14] The OOMMF code is available at http://math.nist.gov/oommf
[15] A. Himeno, T. Okuno, T. Ono, K. Mibu, S. Nasu, and T. Shinjo, J. Magn. Magn. Mater. **286**, 167 (2005).